

## Article

# Study on Application of Comprehensive Geophysical Prospecting Method in Urban Geological Survey—Taking Concealed Bedrock Detection as an Example in Dingcheng District, Changde City, Hunan Province, China

Yu-Long Lu <sup>1</sup>, Chuang-Hua Cao <sup>2,\*</sup>, Yao-Qi Liu <sup>1</sup> and Yang Liu <sup>1</sup><sup>1</sup> School of Earth Sciences and Spatial Information, Hunan University of Science and Technology, Xiangtan 410201, China<sup>2</sup> Institute of Geological Survey of Hunan Province, Changsha 410083, China

\* Correspondence: 21010103009@mail.hnust.edu.cn

**Abstract:** In order to ascertain the concealed bedrock and its spatial distribution in an urban low-resistance coverage area of a typical lacustrine basin in Hunan Province, a multi-method comprehensive experimental study was carried out in Dingcheng District, Changde City where there are multiple sets of strata and fault structures. In this study, the wide-area electromagnetic method and microtremor survey were utilized on the basis of traditional methods, including the high-density resistivity method and controlled-source audio-frequency magnetotelluric method, to infer the concealed Cambrian limestone, fault structure, and vertical distribution of strata and the results were verified by drilling. The results indicate that the wide-area electromagnetic method is effective to explore the bedrock and concealed structure in urban geological survey. The microtremor method has an obvious effect on the detection of the Cretaceous and Quaternary silty strata within 100 m. The study may provide references for similar projects in this area.

**Keywords:** urban geological survey; comprehensive geophysical method; wide-area electromagnetic method; microtremor survey; bedrock survey

**Citation:** Lu, Y.-L.; Cao, C.-H.; Liu, Y.-Q.; Liu, Y. Study on Application of Comprehensive Geophysical Prospecting Method in Urban Geological Survey—Taking Concealed Bedrock Detection as an Example in Dingcheng District, Changde City, Hunan Province, China. *Appl. Sci.* **2023**, *13*, 417. <https://doi.org/10.3390/app13010417>

Academic Editors: Yanlin Zhao, Yixian Wang, Yu Chen, Hang Lin and Rihong Cao

Received: 21 November 2022

Revised: 21 December 2022

Accepted: 23 December 2022

Published: 28 December 2022



**Copyright:** © 2022 by the authors. Licensee MDPI, Basel, Switzerland. This article is an open access article distributed under the terms and conditions of the Creative Commons Attribution (CC BY) license (<https://creativecommons.org/licenses/by/4.0/>).

## 1. Introduction

Since the Ministry of Natural Resources of the People's Republic of China issued "Notice on strengthening urban geological survey" in 2017 [1], a series of urban geological survey work was deployed by the Ministry of Natural Resources and China Geological Survey at the national level as well as the Department of Natural Resources and the geological industry management department at the provincial level. The Ministry of Natural Resources issued the code for urban geological investigation [2] at the end of 2017, the contents involving the geophysical exploration work mainly are as follows: (1) exploration of basic geological conditions in cities; (2) survey and evaluation on urban natural resources; (3) survey and evaluation on the urban geological environment; and (4) urban geological disaster investigation.

Urban geological survey is the predecessor activity of urban development as well as being the basis of urban space's effective and comprehensive utilization. Since the survey of territorial resources in 1999 [3], urban geological work is getting more and more meticulous, and presents a rapid development trend. Environmental geology survey and evaluation of major cities (group) in China have been accomplished, led by the Ministry of Natural Resources and the China Geological Survey. Three-dimensional urban geological surveys were carried out and the underground three-dimensional structure of the city

was established. A three-dimensional visualization urban geological information management decision platform and a public-facing urban geological information service system were also established. From 2004 to 2012 [3], the Ministry of Natural Resources and the China Geological Survey completed environmental geological surveys in major cities all over the country. The investigation preliminarily identified different kinds of urban environmental geological problems including landslide, collapse, debris flow, land subsidence, soil and water pollution, active faults, mine geological environment problems, and the state of geological resources such as groundwater, geothermal, mineral water, and geological landscape was clarified. Since 2009 [3], under the unified deployment of the Ministry of Land and Resources, the multi-party cooperation mode of ministry, province, and city has been adopted to carry out urban geological surveys of 28 cities, including Fuzhou, Xiamen, Quanzhou, Suzhou, Zhenjiang, Jiaxing, Hefei, Shijiazhuang, Tangshan, Qinhuangdao, and Jinan among their number. Since 2010 [3], in order to serve the needs of the national regional strategy and main function zoning, comprehensive geological surveys have been carried out in key urban agglomerations such as Beijing-Tianjin-Hebei, Yangtze River Delta, Pearl River Delta, the west coast of Taiwan Strait, Beibu Gulf, middle reaches of Yangtze River, Guanzhong, Central Plains, and Chengdu-Chongqing. Hunan province has also cooperated with the Ministry of Natural Resources in recent years; since July 2008 [3], the Hunan Provincial Institute of Geological Survey has undertaken a comprehensive survey and regionalization of the geological environment of the Changsha-Zhuzhou-Xiangtan Urban agglomeration, hydraulic and environmental geological survey of Changsha-Zhuzhou-Xiangtan Urban agglomeration and other projects. At present, Changde city geological environment survey, Yiyang city geological environment survey and Yueyang city geological survey projects are in progress. With the deepening of urban geological survey in recent years, geophysical exploration technology has also made some scientific and technological achievements. As early as 1993, Wu Yifang et al. [4] used an electric method, a magnetic method, the creation of an artificial earthquake and other methods to conduct multi-method detection tests on the large area of ground fissure and collapse in Changjiang Road, Tongling City, the results indicating that shallow seismic exploration was the most effective method. In 2007, Chen Xiangfu and An Xifeng [5] took the Guangzhou urban geological survey as an example and pointed out that it was feasible to use seismic transverse wave exploration combined with wave velocity logging to divide the sequence of Quaternary unconsolidated strata and detect the thickness. In 2008, Li Xiaobin et al. [6] confirmed that geophysical exploration has a good application prospect in urban geological surveys through the examples of gravity, magnetic, electric, seismic, and radioactive exploration. In 2015, Yang Qiyan et al. [7] evaluated the Shigatse urban active fault by using a shallow seismic exploration method with a ramming source as the artificial source. In 2017, Han Shuhe et al. [8] used a three-dimensional earthquake, controlled-source audio-frequency magnetotelluric and transient electromagnetic method to comprehensively detect the goaf of the Chifeng Coal Mine. In 2019, Chen Shi et al. [9,10] conducted investigation and application research in Urumchi by using a high-density resistivity method and a natural source surface wave microtremor exploration method, which has guiding significance for the later exploration of urban underground space resources. Jiang Bo et al. [10] used controlled-source audio-magnetotelluric, high-density resistivity, transient electromagnetic and geological radar methods to detect the distribution positions of major fault zones and ancient river channels in Xuzhou city. Wang Yahui et al. [11] explored and modeled the urban underground space in the Xixian New Area of Xi'an by using a comprehensive geophysical exploration method. Zhou Lei and Cao Chuanghua et al. [12] conducted an experimental study on prospecting water using geophysical methods under urban limited site conditions in Chenzhou City, Hunan province through an equivalent retroflux transient electromagnetic method. This paper aims to carry out exploration experiments on the underlying bedrock structure of the urban electrical low resistivity overburden in Huxiang Basin in order to provide experiences for geophysical prospecting application in urban geological survey.

## 2. Geology

The study area is located in the southwest margin of Dongting Basin [13–15], geographically located in the industrial development zone of Dingcheng District, Changde City. The Taiyangshan uplift, Wuling uplift, and Yuan River are in the east, west and south of the experimental profile. The river system in the area is relatively developed, and the exposed stratum is relatively simple in the study area.

### 2.1. Stratum

According to regional geological data, the strata exposed on the surface of the research area are mainly pre-Quaternary bedrock (including Qingbaikou Qb~Paleogene E), Quaternary lower Pleistocene series Changde formation, Quaternary middle Pleistocene series Mawangdui formation, and Quaternary Holocene series. The main stratum is briefly described as follows:

#### (1) Pre-Quaternary bedrock (Qb-E)

Changde city and its periphery are covered by Quaternary bedrock, therefore the Paleogene systems of Proterozoic, Paleozoic, Mesozoic, and Cenozoic are considered as pre-Quaternary bedrock in this study. The Qingbaikou system is the oldest stratum exposed in the survey area, and this includes the Lengjiaxi and Banxi groups distributed in the north of the investigation area located in the Taiyangshan area of Dingcheng District, Changdeding City. The Nanhua and Sinian system are only distributed in Taiyangshan. Cambrian, distributed in the northwest, is the most widely distributed stratum in the survey area. Cambrian stratum is concentrated to the east of Shibatan Town, such as Liantai-Huaishugang-Tiejiazui-Guanshiyan, and in the west of Guanxi Town, in places such as Matousi-Fengjiaqiao-Zhangshuwan, Taiping-Gongjiawan-Lijia-Nanyan. There is a small amount of Cambrian distributed in the Liujiapo area of Chou Town. The Ordovician is distributed in the northwest corner of the survey area, mainly in the NW-trending band in Jinjishan-Zhaojiawan of Shibatan Town, and the Zhoujia-Zhaizishan-Changlinggang reservoir of Guanxi Town. Cretaceous is concentrated in the northwest of Guanxi Town, in places such as Shuomudang-Fujiashan and Wujiawan-Baozhengwan, and there are scattered outcrops in the Quaternary distribution area. Paleogene is concentrated in the N-NE of Liuye Lake in Changde City, namely in the Huangjiachong-Shiiwan-Xiaowupu area.

#### (2) Quaternary lower Pleistocene series Changde formation (Qp<sub>1cd</sub>)

It is mainly distributed in the hilly-to-hilly land morphologic province, which spreads in planar or banded form. It is specifically distributed in Hefu-Guanxi town and the Dingjiagang-Doum Lake-Caoping area. The stratum elevation is generally 60 ~ 120 m, and the sediment is generally 10 ~ 30 m thick, with a maximum thickness of up to 70 m. The lithology is mainly a gravel layer with a small amount of lentoid sand and clay layer. The thickness of the sediment varies frequently from bottom to top, and the phenomenon of internal scour and filling, erosion, and cutting is very common. It is the alluvial-diluvial fan body mainly composed of braided river deposits, with a small amount of debris flow deposits inside.

#### (3) Quaternary middle Pleistocene series Mawangdui formation (Qp<sub>2mw</sub>)

It is distributed in hilly, hilly land, undulating plains and other areas. The elevation is 40~150 m, and the thickness of the stratum varies greatly from 3 to 20 m. Generally, the thickness increases at the place where the geomorphic change occurs. The lithology is mainly brownish red, brownish yellow reticulate clay, containing (weak) reticulate iron-manganese clay; reticulate gravel clay is commonly distributed at the bottom. It is in unconformable contact with the lower strata (Changde formation, Baishajing formation, etc.), which is usually covered at a small angle or cut into the lower sand and gravel layer at a large angle.

#### (4) Quaternary Holocene series (Qh)

It is developed in modern river gullies in relatively low topography areas, and the stratum is distributed in relatively limited areas with a small thickness of 2–9 m. Many of them have a river dual structure with a gravel layer at the lower level and a silty clay layer at the upper.

Deep in the area, there is the Ordovician Baishuixi formation, Cambrian Tanxi formation, Wunitang formation, Niutitang formation, and other strata as follows:

(5) Ordovician Baishuixi Formation ( $O_1bs$ )

The lithology of this formation is mainly composed of grayish yellow to light grayish green thin to medium silty mudstone, locally intercalated with silty mudstone, mudstone, and banded mudstone. This formation is intercalated with an argillaceous limestone lens at the bottom, and intercalated with silty shale in the middle.

(6) Cambrian Tanxi Formation ( $\epsilon_{3-4t}$ )

The lithologic association is mainly composed of calcarenite, calcisiltite, micritic argillaceous limestone, microcrystalline calcite dolomite, and plate-like shale, which is in conformable contact with the underlying Wunitang formation.

(7) Cambrian Wunitang Formation ( $\epsilon_{2-3w}$ )

The formation is characterized by middle-thin-layered micritic argillaceous limestone, banded crystal powder limestone, calcisiltite limestone mixed with calcareous mudstone, mudstone, and calcareous shale. It is in conformable contact with the underlying Niutitang formation, and scattered outcrops are occasionally seen in Liaojiawan, Guanxi Town.

(8) Cambrian Niutitang Formation ( $\epsilon_{1-2n}$ )

This formation is a set of dark gray, gray-black (including) carbonaceous shale, banded carbonaceous shale, carbonaceous mudstone, thin-thick layered carbonaceous mudstone, carbonaceous siliceous mudstone, siliceous carbonaceous mudstone, mudstone-intercalated silty, calcareous shales and lentoid, stratiform-like siliceous rocks.

## 2.2. Geologic Structure

The pre-Quaternary fault structures are mainly distributed in the Taiyangshan-Matoushan area in the northwest of the study area, and are mainly formed in the Indosinian, Yanshan, and Paleogene periods. Since the pre-Quaternary strata are distributed in the north of the survey area, all the pre-Quaternary faults are also distributed in the north of the survey area. The NNE faults are mainly distributed at both sides of the Yangshan uplift. They are featured with a large-scale, eye-catching tectonic track and multi-period activities, which are the product of regional stress fields or confined stress fields in different periods. The NEE and NE faults are on a small scale, they are also cut and restricted by the NNE faults. The structure near the test section is mainly represented by F3 as shown in Figure 1.

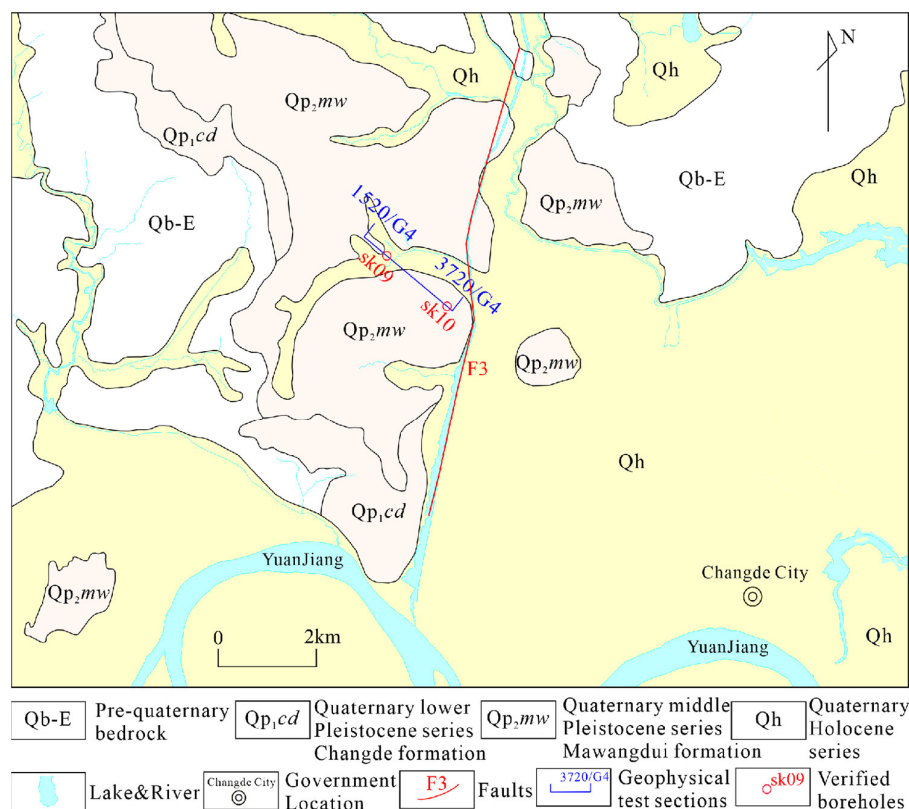


**Figure 1.** Location map of geological and geophysical test sections in the study area (revised from 1:50,000 Chang-de regional geological map).

The Hefu-Shibantan fault (F3) is a relatively large fault on the west side of Taiyangshan, extending from Hefu to Shibantan along the Jian River. In the study area, the extended length is 18.5 km with striking at NE10°~15° and the fault is oriented to the south-east with an inclination angle at about 50°~70°, which is a normal fault with strike-slip. The fault shows a straight deep trench or valley topography, and obvious differences in topography and strata on both sides of the fault. On the east side, the side of residual deposits at the western piedmont of Taiyangshan, the river system is not developed. The west side of the fault is a hilly landform, which is an alluvial fan composed of sand and gravel layers in the early Pleistocene. The Pinnate river system is developed in a vertical-to-fault strike direction.

### 3. Geophysical Techniques and Geophysical Characteristics

#### 3.1. Geophysical Techniques

On the basis of preliminary investigation and research, this application test research follows the working idea of “from the outside to the inside, from the shallow to the deep and step by step”. Firstly, the shallow detection uses the high-density resistivity method, and then the middle and deep detection uses the controlled-source audio-frequency magnetotelluric method. In the later period, the wide-area electromagnetic method was introduced to carry out deep detection for comparative tests. Finally, a new method of natural field wave microtremor was used to detect and analyze the seismic wave velocity and physical properties at the proposed drilling location.

##### 3.1.1. High-Density Resistivity Method

The high-density resistivity method is an improvement of the traditional electrical sounding method. It has high field data collection efficiency and is most widely used in

urban geological survey. In this study, in order to detect the formation structure within 100 m of the shallow layer near the surface, the point distance is selected at 10 m, and 60 electrodes are arranged in a row, at a total distance of 600 m, and the continuous rolling mode is implemented. The acquired parameter is the apparent resistivity, because the apparent resistivity is the overall response of formation information; Res2Dinv software is used to invert the results, in which finite difference is used for forward calculation, and the least square method based on the smooth constraint is used for inversion. The WGMD-4 resistivity data acquisition system developed by the Chongqing Pentium Numerical Control Technology Research Institute was used in this study. A Wenner device with a high longitudinal resolution was selected [16] in order to detect stratum stratification.

### 3.1.2. The Controlled-Source Audio-Magnetotelluric Method

Because the detection depth did not penetrate the low resistance overburden, the controllable source audio-frequency magnetotelluric method was completed on the basis of the detection profile and high-density electrical method. The controlled-source audio-frequency magnetotelluric method (CSAMT) is developed based on magnetotelluric exploration using an artificial source method with frequency domain sounding, the signal strength is large with a detecting depth of 1.5 km, but it is commonly used for “far” area data when dealing with field measured data; thus, its transceiver distance setting is one of the preconditions for effective use of the method. The profile is consistent with the high-density electrical method, with a distance of 20 m. Based on the new understanding of Cao Chuanghua et al. [17] in 2017 regarding the geological survey project of the Changsha-Zhuzhou-Xiangtan urban agglomeration, the power supply AB is arranged in the southwest section of the survey line near Yangjiaxiang Village, Chou Town. The power supply line AB is 1.04 km long, parallel to the profile of the measuring line, and the transmission distance is 9.8 km. The observation device is in TM mode, and the instrument is a GDP32 series multi-functional electrical workstation developed by the Zonge Company in the United States. The generator transmitting power is 30 kW. The emission current presents the characteristics of high frequency with low current and low frequency with high current. The maximum emission current is 16 A and the minimum emission current is 3.5 A. The data collection frequency is 0.125–8192 Hz, and the data processing software uses Scs2D. The processing process includes flying point elimination, static correction, terrain correction and inversion, etc. In this study, one-dimensional Bostick inversion results are used as the initial model of the two-dimensional Occam inversion method.

### 3.1.3. Wide-Area Electromagnetic Method

The wide-area electromagnetic method is a new electromagnetic detection technology developed in the early 21st century, which was invented by academician He Jishan from Central South University. Based on the precise expression of the electromagnetic field, the apparent resistivity parameters of the wide-area electromagnetic method are strictly defined, and the distortion effect in the distant region is improved. Therefore, the sounding can be carried out over a wide area, not limited to the “far zone”, and the exploration depth is larger under the condition of the same transceiver distance. This method inherits the advantages of using a human field source in the CSAMT and magnetic dipole source frequency sounding method (MELOS) with “not far zone” detection. The weakness of the CSAMT remote signal is improved, the range of observation is expanded, and the correction method of the MELOS method is abandoned. A formula suitable for the whole field is used to calculate the apparent resistivity, which retains the high-order term of the calculation formula, greatly expands the observation range of the artificial source electromagnetic method, and improves the observation speed, accuracy, and field efficiency [18]. In this study, the data collected by the controlled-source audio-frequency magnetotelluric method is used to invert the resistivity of the whole area only using electric field scalar and geoelectric field observation parameters without track data, and the frequency is 0.125 Hz–8192 Hz.

### 3.1.4. Natural Source Surface Wave Microtremor

There is a weak continuous natural surface wave signal source in the human activity area near the earth's surface, scholars have used it to detect and calculate the seismic velocity structure of the stratum since the 1950s. At present, low-frequency signals generated by tides, waves, pressure changes and high-frequency mechanical vibration signals generated by human activities are mainly used to deduce the subsurface transverse wave velocity model based on the dispersion curve inversion of these Rayleigh surface wave characteristics [10]. In this study, a WD-1 intelligent natural source surface wave data acquisition system funded by the Beijing Institute of Hydroelectricity Geophysical Exploration was used. Data collection was carried out using a 2 Hz detector 10-channel equilateral triangle embedded pole mode. The maximum side length is 90 m, the sampling interval is 5 m and the number of iterations is 600.

## 3.2. Geophysical Characteristics of the Study Area

### 3.2.1. Regional Geophysical Characteristics of Changde City

The 1:500,000 gravity measurement data of the region shows that the study area is located at the eastern and southwestern edges where the gravity is high, within the Mayang-Changde-Xiangtan-Hengyang arc. Bouguer gravity abnormal values are  $(-50 \sim -10) \times 10^{-5} \text{ m/s}^2$ . The arc gravity height is consistent with the outline of the Mesozoic red bed basin, and has a large mass deficit relative to the basement, which mainly reflects the uplift of the metamorphic crystalline basement and Moho surface [19,20].

The aeromagnetic background field in the study area is  $\Delta T$  positive anomaly, and  $\Delta T$  abnormal values vary from 15 nT to 40 nT. Aeromagnetic  $\Delta T$  anomaly is generally small in the northwest and northeast. From north to south, the  $\Delta T$  anomaly gradient gets smaller and smaller. Aeromagnetic anomaly contour lines bulge from the middle to the northwest and northeast directions. The directions of aeromagnetic anomaly contour lines in the survey area are not in harmony with the strata and tectonic strike lines, indicating that the Quaternary strata exposed in the survey area have the characteristics of a low and slow magnetic field or they have no magnetic field.

The study area is located in the Changde mantle-uplift district, which includes the whole Dongting Lake area. The Changde-Anren transition fault zone divides it into two local mantle-uplift districts, namely Yuanjiang and Taoyuan, with completely different strike directions. The study area is located between two secondary mantle-uplift districts. The Changde-Anren transition fault zone spreads in a northwest direction from the middle of the study area. The buried depth of the Moho surface is 31 ~ 32 km, and the two mantle-uplift districts correspond to the Mesozoic Dongting basin.

### 3.2.2. Petrophysical Characteristics of the Study Area

The four detection methods in this test involve two kinds of parameters, namely electrical parameter resistivity and wave velocity.

The resistivity statistics of different formations in the region are shown in Table 1, and their electrical characteristics are as follows: Quaternary Holocene, Quaternary middle Pleistocene series Mawangdui formation, and Quaternary lower Pleistocene series Changde formation. All of these formations have relatively low resistivity characteristics. The average value is generally less than 300  $\Omega \cdot \text{m}$ , and the resistivity is relatively higher when containing more gravel, while more silty clay content leads to lower resistivity. The average resistivity of silty shale in the Ordovician Baishuixi formation in this area is 1000.3  $\Omega \cdot \text{m}$ , and it is buried deep in this area with less water content, showing moderate resistivity characteristics. The Dolomitic limestone of the Cambrian Tanxi formation has the highest resistivity within the range of detection depth in the study area. The average value is 2788.5  $\Omega \cdot \text{m}$ . The relative resistivity of micritic argillaceous limestone in the Cambrian Winitang formation is lower, with an average value of 1757.3  $\Omega \cdot \text{m}$ . The resistivity is lower than that of the Tanxi formation because of its Argillaceous components. However, the

resistivity of the Cambrian Niutitang formation, with an average value of 798.2Ω·m, is sharply lower than that of other Cambrian strata in the area due to the carbonaceous content. When there are fault structures in the concealed strata, Quaternary bedrock has a natural surface water infiltration channel of the Huxiang Basin, thus presenting locally low resistivity characteristics [21–26]. Different strata have different physical properties. Resistivity parameter detection can be used to detect the buried pre-Quaternary bedrock in the area, which can be used to delineate geological anomalies such as structures.

**Table 1.** Resistivity characteristics of different strata in the study area.

Stratigraphic Code	Rock	Number	Average Resistivity/ $R_{av}$ (Ω·m)	Range/ (Ω·m)
Qb-E	pre-Quaternary bedrock	32	998.3	212.3~5998.8
Qp <sub>1cd</sub>	lower Pleistocene series Changde formation conglomerate	22	223.1	128.3~889.5
Qp <sub>2mw</sub>	middle Pleistocene series Mawangdui formation reticular clay	33	23.1	100.5~2122.9
Qh	Quaternary Holocene series gravel layer, silty clay	27	298.3	12.5~588.7
O <sub>1bs</sub>	Ordovician Baishuixi formation silty shale	36	1000.3	621.9~1768.5
Є <sub>3-4t</sub>	Cambrian Tanxi formation dolomitic limestone	31	2788.5	1189.3~5998.8
Є <sub>2-3w</sub>	Cambrian Wunidtang formation micritic argillaceous limestone	33	1757.3	1121.1~2678.3
Є <sub>1-2n</sub>	Cambrian Niutitang formation Carbonaceous shale and mudstone	35	798.2	339.1~1233.5

The transverse wave velocity range of different strata in the area is shown in Table 2. The exposed strata in the site are mainly Quaternary. The surface clay within 100 m, conglomerates, and pre-Quaternary bedrock have significant differences in wave velocity, especially gravel-bearing strata within Quaternary that can be effectively distinguished, indicating that there are preconditions for developing natural surface waves in this area.

**Table 2.** S-wave velocity range of different strata in the study area.

Stratigraphic Code	Rock	Transverse Wave Velocity/ $V_{tw}$ (m·s <sup>-1</sup> )
Qb-E	pre-Quaternary bedrock	>800
Qp <sub>1cd</sub>	lower Pleistocene series Changde formation conglomerate	300~700
Qp <sub>2mw</sub>	middle Pleistocene series Mawangdui formation reticular clay	<300
Qh	Quaternary Holocene series gravel layer, silty clay	300~800
O <sub>1bs</sub>	Ordovician Baishuixi formation silty shale	700~900
Є <sub>3-4t</sub>	Cambrian Tanxi formation dolomitic limestone	>1300
Є <sub>2-3w</sub>	Cambrian Wunidtang formation micritic argillaceous limestone	>1100
Є <sub>1-2n</sub>	Cambrian Niutitang formation Carbonaceous shale and mudstone	>900

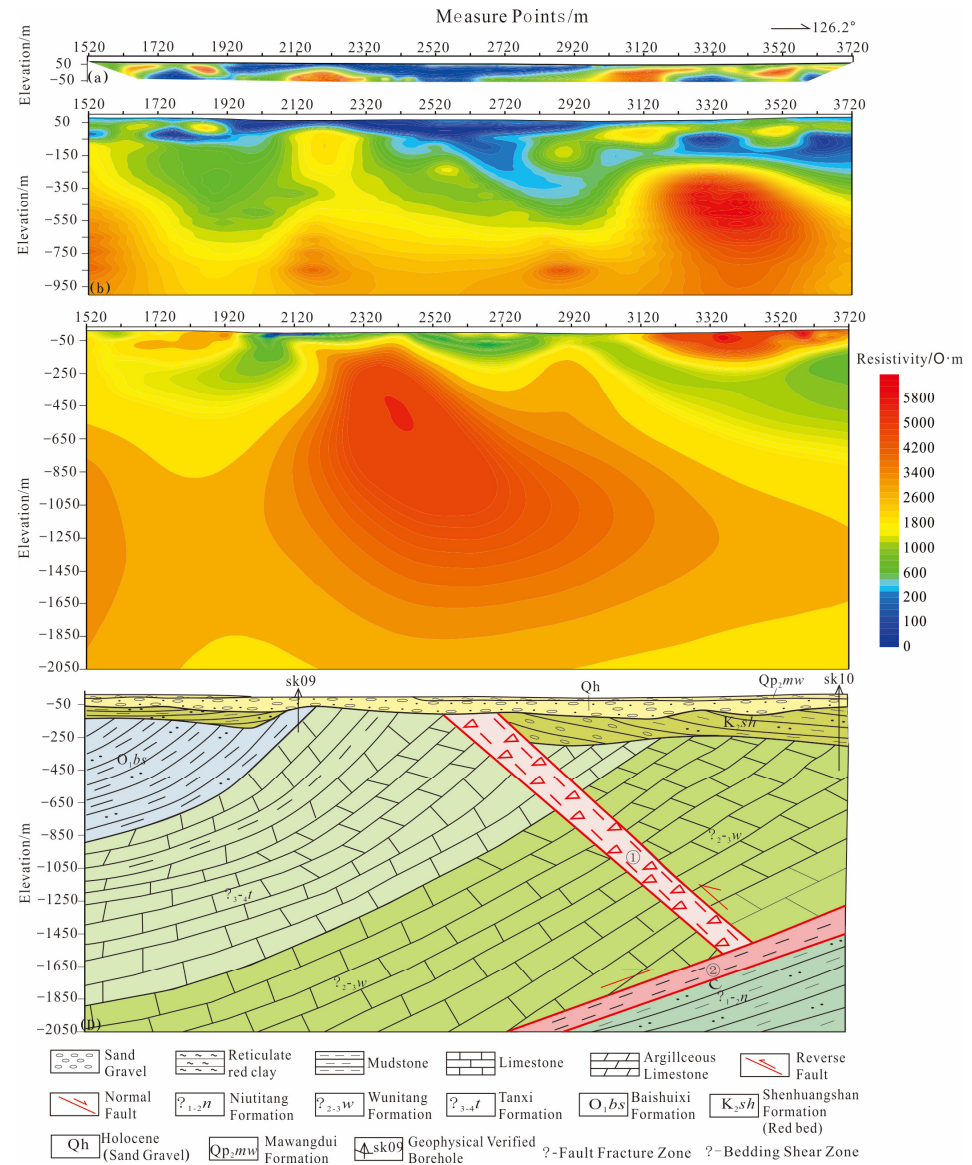
## 4. Results Interpretation and Drilling Verification

### 4.1. Results Interpretation

According to the input format requirements of the Res2Dinv software, the original data of the designed G4 section that was obtained from the high-density electrical method are spliced and sorted into an independent data file. The least square method based on the smooth constraint was used for inversion, and the results in Figure 2a were obtained after terrain correction. The resistivity of the whole section is low above the altitude of −50



m, generally less than 2000  $\Omega\cdot\text{m}$ . Combined with the survey results of surface geological mapping, it is inferred that most of them belong to Quaternary, and the low resistivity characteristics are relatively continuous. Based on the results of Table 1, it can be inferred that it is middle Pleistocene series Mawangdui formation reticular clay, and the underlying layer is a Quaternary Holocene gravel layer before 1920 measure points and after 2450 measure points when the surface.



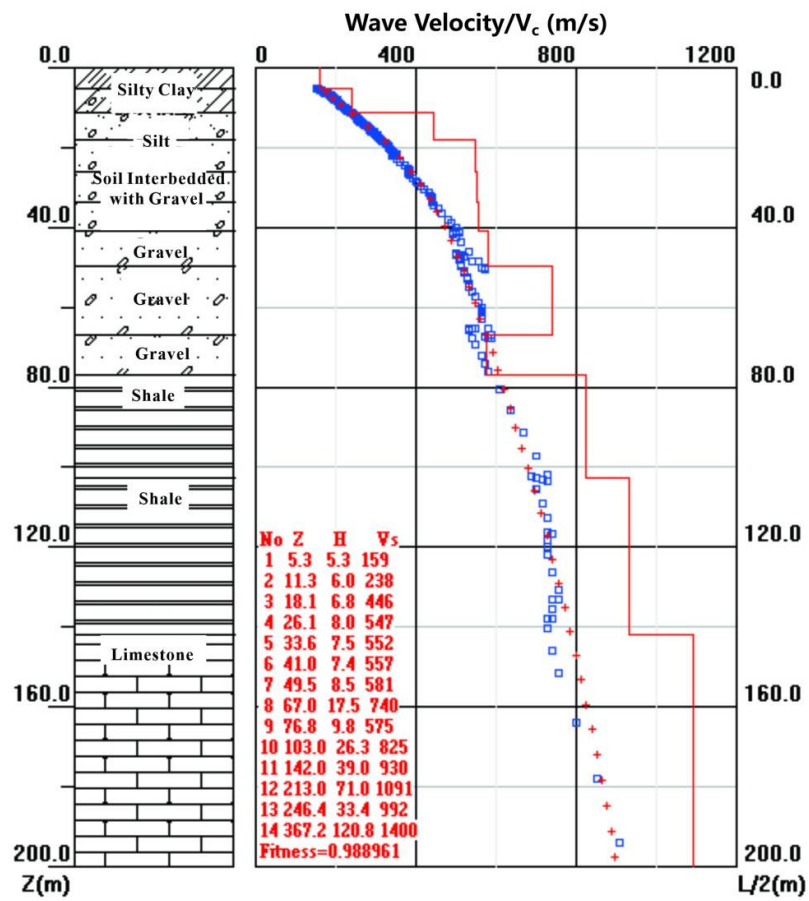
**Figure 2.** Geological interpretation of G4 test profile in the study area (a) High-density electrical processing results; (b) Controllable-source audio-magnetotelluric processing results; (c) Wide-area electromagnetic processing results; (d) Geological profile of G4.

Figure 2b shows the data processing results of the controlled-source audio-frequency magnetotelluric method. Stratum stratification is obvious and can be divided into three layers. The first layer is a low resistivity layer with an altitude above  $-100$  m, and the resistivity is generally less than 2000  $\Omega\cdot\text{m}$ . The second layer is a medium resistivity resistance layer over  $-550$  m above sea level, but it presents two depressions similar to a faulted basin. The first is located between 1650 and 2120 measure points and the other

between 2320 and 2920 measure points. The resistivity of the first depression has no obvious zonal distribution characteristics and the resistivity step changes slowly, which is inferred to be caused by the stratum. In the second depression, a low resistivity zone, extending in an east-southeast direction, has an obvious resistivity step zone change. It is inferred that the structure in the deep bedrock is of low resistivity due to the water leakage developed in the shallow surface. The deep strata between  $-650\sim-950$  altitude are characterized by a high resistivity, which can be inferred to be Cambrian limestone, dolomitic limestone, and other strata. However, it is worth noting that there are several small closed anomalies in the shape of a “bull’s eye” in the inversion profile with the controlled-source audio magnetotelluric method, and the distribution is irregular, such as 2520–2620 measure point altitude  $-200$  and 2820–2920 measure point altitude  $-150$  m. It is confirmed that the controlled-source audio-frequency magnetotelluric method is seriously disturbed by the magnetic field in an urban area, which causes the jump of the electromagnetic field signal, a fact that may bring inconvenience to interpretation.

In order to further strengthen the geological understanding of the test section, the electric field data collected by GDP32 and processed by Professor Liu Chunming from Central South University were used to obtain the data processing results of the wide-area electromagnetic method, as shown in Figure 2c. It is obvious that the graph data is smooth and stable, and the stratification is also more obvious. Combined with the previous two methods, the section is interpreted comprehensively, and the results are shown in Figure 2d. It is Quaternary above  $-100$  m and there is only a high resistance at the large measure point between 3220 and 3720. According to the field investigation, it may be interfered by the industrial stray current in the shallow surface because the data were collected at the roadside of an industrial development zone where human activities are concentrated. The Cretaceous strata underlying Quaternary show relatively moderate resistivity at around  $600\ \Omega\cdot\text{m}$ . The middle part is relatively missing, and it is inferred that there are Cretaceous strata before the 2120 measure point and after the 2720 measure point. The middle measure points between 2120 and 2520 are arched by the high resistivity body of the section, which is inferred to be Cambrian strata, and the top of which is in unconformable contact with Quaternary in deep Cambrian strata. In combination with the results of the regional geological survey, it is inferred that there is a fault fracture zone with a width of about 80 m and a southeast dip in the depth of the 2520 measure point. The dolomitic limestone of the Tanxi formation and the micrite argillaceous limestone of the Wunitang formation were transformed by tectonic movement. In the deep and on the southeast of the fault, Cambrian Niutitang formation carboniferous strata exist with a dip angle of about  $30^\circ$  and a lean to the northwest.

It can be seen based on the above results that the resistivity detection method has a good resolution for identifying large geological structures and stratum distribution, but it is difficult to figure out more detailed stratification within the Quaternary, which is the more prominent in the Dongting Basin Changde area where the typical water system of the Huxiang Basin developed. In order to provide multi-parameter information for bedrock detection, natural surface wave microtremor detection was completed in the vicinity of a sk09 verification borehole (measure point 2120) and sk10 (measure point 3700), respectively. The detection results are shown in Figures 3 and 4.



**Figure 3.** Lithographic layering results of sk09 natural source surface wave microtremor detection of dispersive wave velocity.

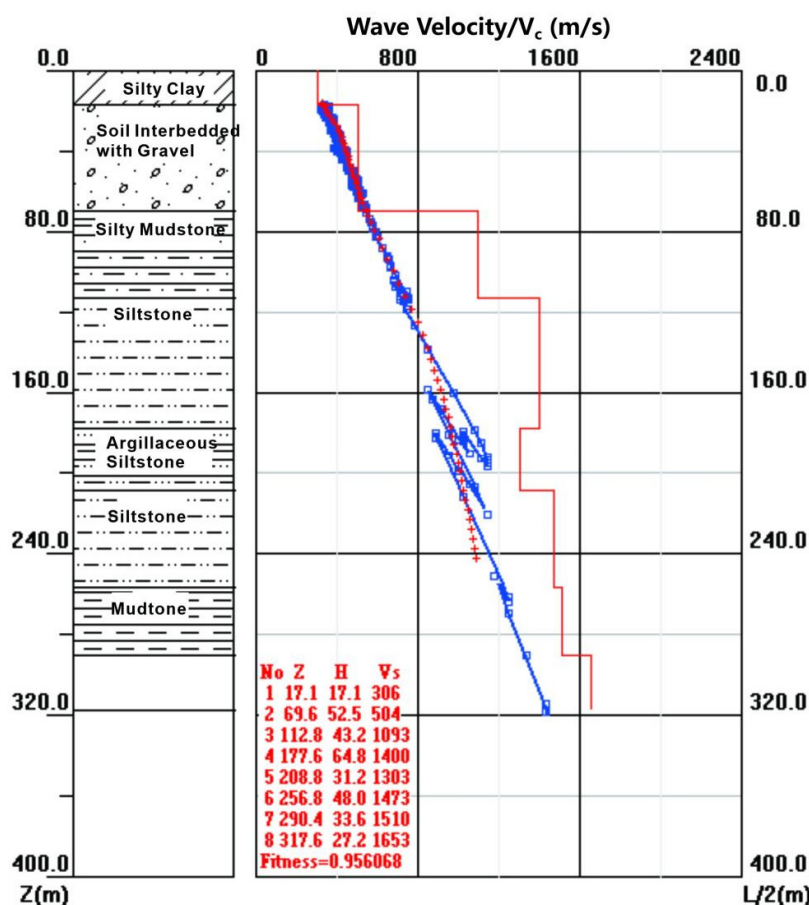


**Figure 4.** Lithographic layering results of sk10 natural source surface wave microtremor detection of dispersive wave velocity.

In the surface wave dispersion curve after inversion, information such as the inflection point of the curve, tangent mutation point of the curve, and wave velocity change are used to stratify the results. Based on the information on the wave velocity difference in Table 2, sk09 can be divided into five layers and sk10 can be divided into eight layers according to comprehensive geological understanding. sk09 inferred that the first layer is silty clay and silty sand with a wave velocity of  $159\text{--}446\text{ m}\cdot\text{s}^{-1}$  above 18 m below the surface. The second layer is a soil-intercalated gravel layer between 40 m and 18 m below the surface, and the wave velocity is between  $547$  and  $581\text{ m}\cdot\text{s}^{-1}$ . The third layer is a pebble layer with a wave velocity of  $575\text{--}740\text{ m}\cdot\text{s}^{-1}$  between 75 and 40 m below the surface. The fourth layer is a shale layer between 145 m and 75 m below the surface, and the wave velocity is between  $825$  m and  $930\text{ m}\cdot\text{s}^{-1}$ . The fifth layer is a limestone layer with a wave velocity of  $992\text{--}1400\text{ m}\cdot\text{s}^{-1}$ , at 145 m below the surface. sk10 inferred that the first layer is a silty clay layer at more than 10 m below the surface, with a wave velocity of  $306\text{ m}\cdot\text{s}^{-1}$ . The second layer is a soil-intercalated gravel layer at 70 m~10 m below the surface, and the wave velocity is  $504\text{ m}\cdot\text{s}^{-1}$ . The third layer is silty mudstone at 110 and 70 m below the surface with a wave velocity of  $1093\text{ m}\cdot\text{s}^{-1}$ . The fourth layer is siltstone with a wave velocity of  $1400\text{ m}\cdot\text{s}^{-1}$  at 180~110 m below the surface. The fifth layer is argillaceous siltstone with a wave velocity of  $1303\text{ m}\cdot\text{s}^{-1}$  at 210~180 m below the surface. The sixth layer is siltstone with a wave velocity of  $1473\text{ m}\cdot\text{s}^{-1}$  at 270 m~210 m below the surface. The seventh layer is mudstone at 310~270 m below the surface with a wave velocity of  $1510\text{ m}\cdot\text{s}^{-1}$ . The eighth layer is limestone at 320~310 m below the surface with a wave velocity of  $1653\text{ m}\cdot\text{s}^{-1}$ .

#### 4.2. Drilling Verification

According to the comprehensive exploration interpretation results in the previous section, drilling verification is carried out on sk09 and sk10 in Figure 1 and Figure 2, respectively. The final hole depth of sk09 is 202.18 m (Figure 5), and that of sk10 is 302.8 m (Figure 6). For sk09, over 89.5 m below the surface is Quaternary, and 3.7 m above is cultivated soil, silty clay is at 3.7 m–18.3 m, and a sandy pebble layer is located between 18.3 m and 89.5 m. The silty shales of the Ordovician Baishuixi formation are at 89.5 m–147.8 m, and the dolomitic limestone of the Cambrian Tanxi formation is located at 147.8 m–202.18 m. For sk10, 9.7 m below the surface is the reticular clay of the middle Pleistocene Mawangdui formation, a Quaternary Holocene gravel layer is located from 9.7 m to 71.52 m below the surface, and a cretaceous red bed is located 71.52 m–275.74 m below the surface. Below 275.74 m, it is the crystalline argillaceous limestone of the Cambrian Wunidtang formation. The drilling results correspond well with the microtremor detection results, especially the inner stratification of low resistivity Quaternary and Cretaceous red beds, which prove to be accurate.

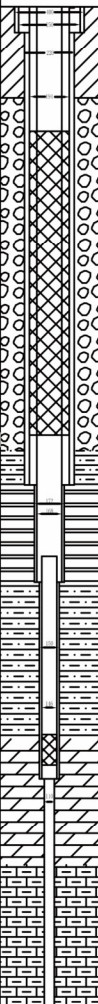
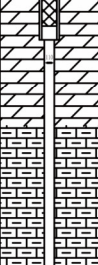
Stratigraphic Unit	Layered Hole Depth (m)	Layered Thickness (m)	Bottom Level (m)	Columnar Section & Borehole Structure	Core Geology Description
Qh	3.70	3.70	49.30		Planting soil, silty clay with a small amount gravel
	18.30	14.80	34.70		Silty clay: grayish yellow, with silty fine-grained sand
	89.50	71.20	36.50		Sand gravel: dark gray and grayish yellow colored; high compactness, good roundness and medium sorting, round-sub-rounded shaped; gravel content is 60%–70%, it is composed mainly by siliceous rock, quartz sandstone and vein quartz; the general particle size is 20–70mm with the maximum size is >100mm; Mud-sand filling, the filling content is more than 30%, containing abundant pore water.
	147.80	58.30	94.80		The color is mainly grayish yellow, brown yellow, brown yellow and yellow white. It is mainly composed by silty shale, shale, argillaceous siltstone. It contains marlstone with poor fissure water at the bottom.
O <sub>1</sub> bs	173.31	25.51	120.31		Marlstone: amaranth, thick-layered; gray, gray-white nodular limestone interbedded with thin argillaceous limestone; karst is quite developed at 148.62–151.20m; dissolution is argillaceous filling, containing small amount karst fissure water.
	202.18	28.87	149.18		Argillaceous limestone: Grey, grey white, thick-layered; karst is not developed and some cracks are calcite veins; argillaceous and ferromanganese filling with small amount karst fissure water.

Figure 5. sk9 drilling core cataloging results.







Stratigraphic Unit	Layered Hole Depth (m)	Layered Thickness (m)	Bottom Level (m)	Columnar Section & Borehole Structure	Core Geology Description
Qp <sub>mw</sub>	3.72	3.72	52.27		0~0.65m planting soil, 0.65~2.65m silty clay: brown yellow, gray yellow, gray white, columnar core, plastic to hard plastic; 26~65-3.72m gravel: gray black, teal gray, dark gray, argillaceous filling; silt content >35%, good roundness, round to sub-rounded shape, slightly denser; the pebble is composed of siliceous rock, silicified limestone, quartz sandstone with poor pore water.
Qh	9.70	5.98	46.29		3.72~6.30m silty clay, grayish yellow, plastic, slightly wet-wet; 6.30~9.70m argillaceous fine sand, brownish yellow, slightly wet-wet, containing poor pore water.  Sandy gravel: gray, gray, dark gray, gray black; dense, medium sorting, poor roundness, sub-circlet to sub-angular flat; the general particle size is 2~5cm, maximum >10cm; fine sand, clay filling, filling content is 30%~35%; gravel, pebbles are composed of siliceous rock, silicified limestone, ferric sandstone, quartz sandstone, quartz veins with rich pore water.
K <sub>2sh</sub>	71.52	61.82	-15.53		71.52~142.55m: calcareous silty mudstone, brick red - brownish red colored, medium weathered - unweathered, the core is relatively complete, the fissure is not developed, basically containing no water. 142.55~148.30m: argillaceous siltstone, brownish red, unweathered; stratified structure, clastic texture, developed fracture with poor pore water. 148.30~167.10m: fine sandstone, brownish red, unweathered, massive structure, clastic texture, developed fracture with poor pore water. 167.10~238.46m: calc-argillaceous siltstone, brownish red, unweathered, stratified structure, pelitic texture; complete core in long column shape, the fissure is not developed, basically containing no water. 238.46~242.50m: fine sandstone, light red, calcium cementing, developed fissures; the core is broken into pieces, stratified structure, clastic texture, developed fracture with poor pore water. 242.50~275.54m: calcium silty mudstone, brick red - brownish red, light red colored, stratified structure, pelitic texture; complete core in long column shape, the fissure is not developed, basically containing no water.  Banded mudstone, dark grey bands alternated with grayish white ones, interbedded with mudstone; stratified structure, pelitic texture; the bands are crumpled and curved, the fissures are argillaceous filled; in 285.20~290.00m, the cores are crushed, mostly mechanical broken, almost without water.
Є <sub>2-3w</sub>	275.74	75.74	-219.75		Banded argillaceous limestone, unpunched, light grey-dark grey, stratified structure, micritic texture; the core is 50% broken and shown in fragmented shape, the rest are long-short columnar shape; karst is not developed, and the fractures are developed along the bedding plane; the fractures are mostly filled with calcite veins, small dissolved pores are developed around the calcite, containing poor pore water.
	297.82	22.08	-241.83		
	302.80	4.98	-149.18		

Figure 6. sk10 drilling core cataloging results.

## 5. Conclusions

Comprehensive geophysical prospecting methods were conducted in the Changde City geological survey. All the traditional methods, including the high-density resistivity and controllable source audio-frequency magnetotelluric methods, have their limitations and deficiencies. Therefore, the wide-area electromagnetic method and natural surface wave microtremor method were introduced in this study to infer the buried strata and faults. The results indicate that the wide-area electromagnetic method could fundamentally reduce signal interference and maximize signal-to-noise ratio; it has a large detection depth and wide frequency band to process inversion. The natural surface wave microtremor method can effectively improve the resolution of near-surface detection in low resistivity coverage areas, and it can be used for exploring the stratified inversion of Quaternary and Cretaceous red beds.

It is necessary to combine the advantages of various methods and use multi-parameter methods to carry out a comprehensive evaluation in any urban geological survey. It is a basic idea that could improve the effect of urban geophysical exploration by comprehensively interpreting geophysical data based on the results of geological survey.

**Author Contributions:** Software, Y.-Q.L.; Writing—original draft, Y.-L.L.; Writing—review & editing, Y.L.; Project administration, C.-H.C. All authors have read and agreed to the published version of the manuscript.

**Funding:** This work was supported by the Research Foundation of the Department of Natural Resources of Hunan Province (Grant No. 2022-25, 2020-04), National Undergraduate Training Program for Innovation and Entrepreneurship (Grant No. S202110534002), Natural Science Foundation of Hunan Province (Grant No. 2022JJ30244), and the Research Project of Teaching Reform of Hunan Province (Grant No. HNJG-2022-0790).

**Institutional Review Board Statement:** Not applicable.

**Informed Consent Statement:** Not applicable.

**Data Availability Statement:** No new data were created or analyzed in this study. Data sharing is not applicable to this article.

**Conflicts of Interest:** The authors declare no conflict of interest.

## References

1. Ministry of Natural Resources of the People's Republic of China. Guiding Opinions on Strengthening Urban Geological Work. 2017. Available online: [http://www.cgs.gov.cn/tzgg/tzgg/201709/t20170906\\_439047.html](http://www.cgs.gov.cn/tzgg/tzgg/201709/t20170906_439047.html) (accessed on July 1<sup>st</sup>, 2017).
2. Ministry of Natural Resources of the People's Republic of China. Announcement of the Ministry of Natural Resources of the People's Republic of China on the Release of Three Industry Standards, Including the "Specifications for Urban Geological Surveys". 2017. Available online: <http://finance.china.com.cn/roll/20170915/4393119.shtml> (accessed on July 1<sup>st</sup>, 2017).
3. Cao, C.H. *Proposal for the Science and Technology Research Project of Hunan Provincial Department of Land and Resources*; Hunan Provincial Geological Survey: Changsha, China, 2017.
4. Wu, Y.F.; Song, W.R.; Xu, H.G.; Liu, J.D. Application of shallow geophysical prospecting in monitoring urban geological hazards. *Hazardology* **1993**, *8*, 27–30.
5. Li, X.B.; Cai, X.M.; Zhao, Y.; Wang, Z.H. Application of geophysical methods in urban geological survey. *Urban Geol.* **2008**, *3*, 31–36.
6. Chen, X.F.; An, X.F. Seismic shear wave exploration and its application in shallow rock and soil layering. *Prog. Geophys.* **2007**, *05*, 1655–1659.
7. Yang, Q.Y.; Peng, Y.Q.; Ni, M.; Gao, J.R.; Wen, S.L.; Zhang, R.Q.; Wu, Q.J.; Lu, G.J.; Wang, Y. Geophysical exploration methods and results of active faults in Shigatse City. *Chin. J. Geophys.* **2015**, *58*, 2137–2147.
8. Han, S.H.; Zhang, S.T.; Guo, Y.F.; Mo, L.T. Application of multiple geophysical methods in the goaf survey. *Nonferrous Met. Eng.* **2017**, *7*, 76–81.
9. Chen, S.; Li, Y.Q.; Li, T.H.; Zhang, J. Application of high-density electrical method in urban basic geological survey. *Xinjiang Geol.* **2019**, *37*, 28–33.
10. Chen, S.; Li, Y.Q.; Li, T.H.; Jin, R.J.; Zhang, J. Application of Natural Source Surface Wave Technology in Urumqi Urban Geological Survey. *Geophys. Geochem. Explor.* **2019**, *43*, 1389–1398.
11. Jiang, B.; Huang, J.J.; Jiang, G.Q.; Zhang, L.; Wu, X.; Xu, S.Y. Application of Geophysical Prospecting Technology in Xuzhou Urban Geological Survey. *Urban Geol.* **2019**, *14*, 101–108.
12. Wang, Y.H.; Zhang, M.S.; Shi, Y.C.; Dong, Y.; Wang, F.; Yu, F.D. Exploration and Modeling of Urban Underground Space Based on Comprehensive Geophysical Prospecting. *Northwestern Geol.* **2019**, *52*, 83–94.
13. Zhou, L.; Cao, C.H.; Deng, Z.; Tan, J.L.; Long, X. Geophysical Prospecting Water Finding Experiments in Limited Urban Sites. *Urban Geol.* **2019**, *14*, 97–102.
14. Liu, G.Y.; Zhao, W.; Wei, F.H.; Luo, L.; Zhao, R.C.; Liang, E.Y. Analysis and sedimentary characteristics of the early Pleistocene gravel formations in the Nandoumu Lake area of Changde, Hunan. *Chin. Geol. Surv.* **2019**, *6*, 68–75.
15. Zhao, Y.L.; Zhang, C.S.; Wang, Y.X.; Lin, H. Shear-related roughness classification and strength model of natural rock joint based on fuzzy comprehensive evaluation. *Int. J. Rock Mech. Min. Sci.* **2020**, *137*, 104550.
16. Zhao, Y.L.; Liu, Q.; Zhang, C.S.; Liao, J.; Lin, H.; Wang, Y.X. Coupled seepage-damage effect in fractured rock masses: Model development and a case study. *Int. J. Rock Mech. Min. Sci.* **2021**, *144*, 104822.
17. Liu, J.X.; Cao, C.H.; Guo, R.W.; Xie, G.F.; Liu, Y. Experimental research on high-density electrical sounding under different devices. *Eng. Surv.* **2013**, *41*, 85–89.
18. Cao, C.H.; Deng, Z.; Liu, J.X. Discussion and Case Analysis of CSAMT Method Transceiver Distance in Changzutan Area. *J. Chin. Nonferrous Met.* **2017**, *27*, 345–355.
19. He, J.S. Combined Application of Wide-Field Electromagnetic Method and Flow Field Fitting Method for High-Resolution Exploration: A Case Study of the An-jia-ling No. 1 Coal Mine. *Engineering* **2018**, *4*, 188–205.
20. Liu, J.H.; Zhao, Y.L.; Tan, T.; Zhang, L.Y.; Zhu, S.T.; Xu, F.Y. Evolution and modeling of mine water inflow and hazards characteristics in southern coalfields of China: A case of Meitanba mine. *Int. J. Min. Sci. Technol.* **2022**, *32*, 513–524.

21. Zhao, Y.L.; Zhang, L.Y.; Liao, J.; Wang, W.J.; Liu, Q.; Tang, L.M. Experimental study of fracture toughness and subcritical crack growth of three rocks under different environments. *Int. J. Geomech.* **2020**, *20*, 4020128.
22. Zhao, Y.L.; Tang, J.Z.; Chen, Y.; Zhang, L.Y.; Wang, W.J.; Liao, J.P. Hydromechanical coupling tests for mechanical and permeability characteristics of fractured limestone in complete stress-strain process. *Environ. Earth Sci.* **2017**, *76*, 24.
23. Zhao, Y.L.; Luo, S.L.; Wang, Y.X.; Wang, W.J.; Zhang, L.Y.; Wan, W. Numerical analysis of karst water inrush and a criterion for establishing the width of water-resistant rock pillars. *Mine Water Environ.* **2017**, *36*, 508–519.
24. Liu, Y.; He, B.C.; Xie, J.; Lu, Y.L.; Zhang, L.Z. Compatibility of geosynthetic clay liners at different temperatures. *J Environ. Prot. Ecol.*, **2021**, *22*, 2295–2306.
25. Zhan, Y.D.; Shao, Y.J.; Liu, Q.Q.; Zhang, X.; Chen, M.H.; Lu, Y.L.; Zhang, Y.C.; Tan, H.J. Hydrothermal rutile U-Pb dating of gold mineralization in the Jiangnan Orogen: A case study of the Hengjiangchong gold deposit in northeastern Hunan. *Ore Geol. Rev.*, **2022**, *149*, 105115.
26. Lu, Y.L.; Li, X.Q.; Liu, Y.; Leng, J.H. The establishment of ore-controlling fracture system of Baoginshan gold mine based on fracture-tectonic analysis. *Mobile Information Systems* 2021, *2*, 1–9.

**Disclaimer/Publisher's Note:** The statements, opinions and data contained in all publications are solely those of the individual author(s) and contributor(s) and not of MDPI and/or the editor(s). MDPI and/or the editor(s) disclaim responsibility for any injury to people or property resulting from any ideas, methods, instructions or products referred to in the content.